





The Potential Significance of the EMILIN3 Gene in Augmenting the Aggressiveness of Low-Grade Gliomas is Noteworthy

Li'ao Wang ¹, Zhiming Zheng ², Jia Zheng², Guifeng Zhang ³, Zheng Wang ⁴

¹Clinical College of Neurology, Neurosurgery and Neurorehabilitation, Tianjin Medical University, Tianjin, 300203, People's Republic of China;

²Department of Neurosurgery, Shandong Provincial Hospital Affiliated to Shandong First Medical University, Jinan, 250021, People's Republic of China;

³Department of Neurology, Liaocheng People's Hospital, Liaocheng, 252004, People's Republic of China; ⁴Department of Neurosurgery, Liaocheng Traditional Chinese Medicine Hospital, Liaocheng, 252000, People's Republic of China

Correspondence: Guifeng Zhang, Department of Neurology, Liaocheng People's Hospital, Liaocheng, 252004, People's Republic of China, Tel +86 18063513155, Email GFZhangNo.1@gmail.com; Zheng Wang, Department of Neurosurgery, Liaocheng Traditional Chinese Medicine Hospital, Liaocheng, 252000, People's Republic of China, Tel +86 18063560328, Email zhengyimingdao@gmail.com

Purpose: Low-grade gliomas (LGG) are common brain tumors with high mortality rates. Cancer cell invasion is a significant factor in tumor metastasis. Novel biomarkers are urgently needed to predict LGG prognosis effectively.

Methods: The data for LGG were obtained from the Bioinformatics database. A consensus clustering analysis was performed to identify molecular subtypes linked with invasion in LGG. Differential expression analysis was performed to identify differentially expressed genes (DEGs) between the identified clusters. Enrichment analyses were then conducted to explore the function for DEGs. Prognostic signatures were placed, and their predictive power was assessed. Furthermore, the invasion-related prognostic signature was validated using the CGGA dataset. Subsequently, clinical specimens were procured in order to validate the expression levels of the distinct genes examined in this research, and to further explore the impact of these genes on the glioma cell line LN229 and HS-683.

Results: Two invasion-related molecular subtypes of LGG were identified, and we sifted 163 DEGs between them. The enrichment analyses indicated that DEGs are mainly related to pattern specification process. Subsequently, 10 signature genes (*IGF2BP2*, *SRY*, *CHI3L1*, *IGF2BP3*, *MEOX2*, *ABCC3*, *HOXC4*, *OTP*, *METTL7B*, and *EMILIN3*) were sifted out to construct a risk model. Besides, the survival (OS) in the high-risk group was lower. The performance of the risk model was verified. Furthermore, a highly reliable nomogram was generated. Cellular experiments revealed the ability to promote cell viability, value-addedness, migratory ability, invasive ability, and colony-forming ability of the glioma cell line LN229 and HS-683. The qRT-PCR analysis of clinical glioma samples showed that these 10 genes were expressed at higher levels in high-grade gliomas than in low-grade gliomas, suggesting that these genes are associated with poor prognosis of gliomas.

Conclusion: Our study sifted out ten invasion-related biomarkers of LGG, providing a reference for treatments and prognostic prediction in LGG.

Keywords: LGG, prognosis, invasion, overall survival, EMILIN3

Introduction

Approximately 30% of primary CNS tumours and 80% of CNS malignancies are gliomas, the most common and malignant primary tumour in adults.¹ These brain glial cell tumours have a high recurrence, short survival, and high fatality rate.² Histopathological malignancy criteria classify gliomas as grades I–IV. Even after full surgical resection, radiation, and chemotherapy, high-grade gliomas (HGGs) survive 4–6 weeks and 12–18 months.³ About 22% of adult brain malignancies are slow-growing, infiltrative, intermittent low-grade gliomas (LGG).⁴ LGG has an overall survival (OS) of 85% at five years but a progression-free survival (PFS) of 40%, which is poor compared to HGGs.^{5,6} Additionally, 70% of LGG patients will advance within ten years, worsening their prognosis.⁷ Thus, new predictive biomarkers with specificity and utility are needed to improve LGG diagnosis, therapy, and prediction.

Aggressive LGG has poor prognosis and high treatment resistance.⁸ Primary invasion by glioma cells occurs in the perivascular space and brain parenchyma.⁹ Several mechanisms contribute to LGG tumour invasion and migration, including EMT, hypoxia, angiogenesis, and the TME.¹⁰ EMT transforms epithelial cells into

mesenchymal cells with altered marker expression.^{11,12} HIF-1 α -regulated hypoxia causes tumour adaptability, progression, and therapeutic resistance, increasing aggressiveness.^{13,14} Solid tumour growth requires angiogenesis, which LGG migration and invasion are connected to.¹⁵ Certain microRNAs affect LGG aggressiveness and angiogenesis during glioma formation.¹⁶ The M2 TAMs enhance glioma development and invasion.^{17,18} LGG migration and invasion are affected by cancer cell metabolism and adhesion molecules.^{19,20} The identification of invasion-related molecular characteristics and markers in LGG may improve prognosis, survival, and treatment.^{21,22}

This paper used a consistent clustering approach in the TCGA-LGG transcriptome dataset based on the invasion-related gene set to divide the LGG samples into two subclasses. We obtained differentially expressed genes between the subclasses. Then, using one-way Cox regression analysis and the LASSO algorithm, we screened ten genes and calculated risk scores to divide the LGG samples into high and low-risk groups. Next, we explored the differences in infiltration levels of immune infiltrating cells, ESTIMATE scores, and immune checkpoints between risk groups, constructed ceRNA networks to explore their upstream and downstream regulatory mechanisms, and finally built a predictive model. PCR testing of clinical samples and EMILIN3 gene function experiments validated our analyses. In summary, these findings provide some theoretical basis for the prognostic assessment of LGG, the development of new therapeutic tools, and the further elucidation of molecular mechanisms associated with invasion. In addition, the genes that make up the risk score can be used as the basis and direction for further research. We analyse the flowchart and some of the results of the article analysis as a study process map (Figure 1).

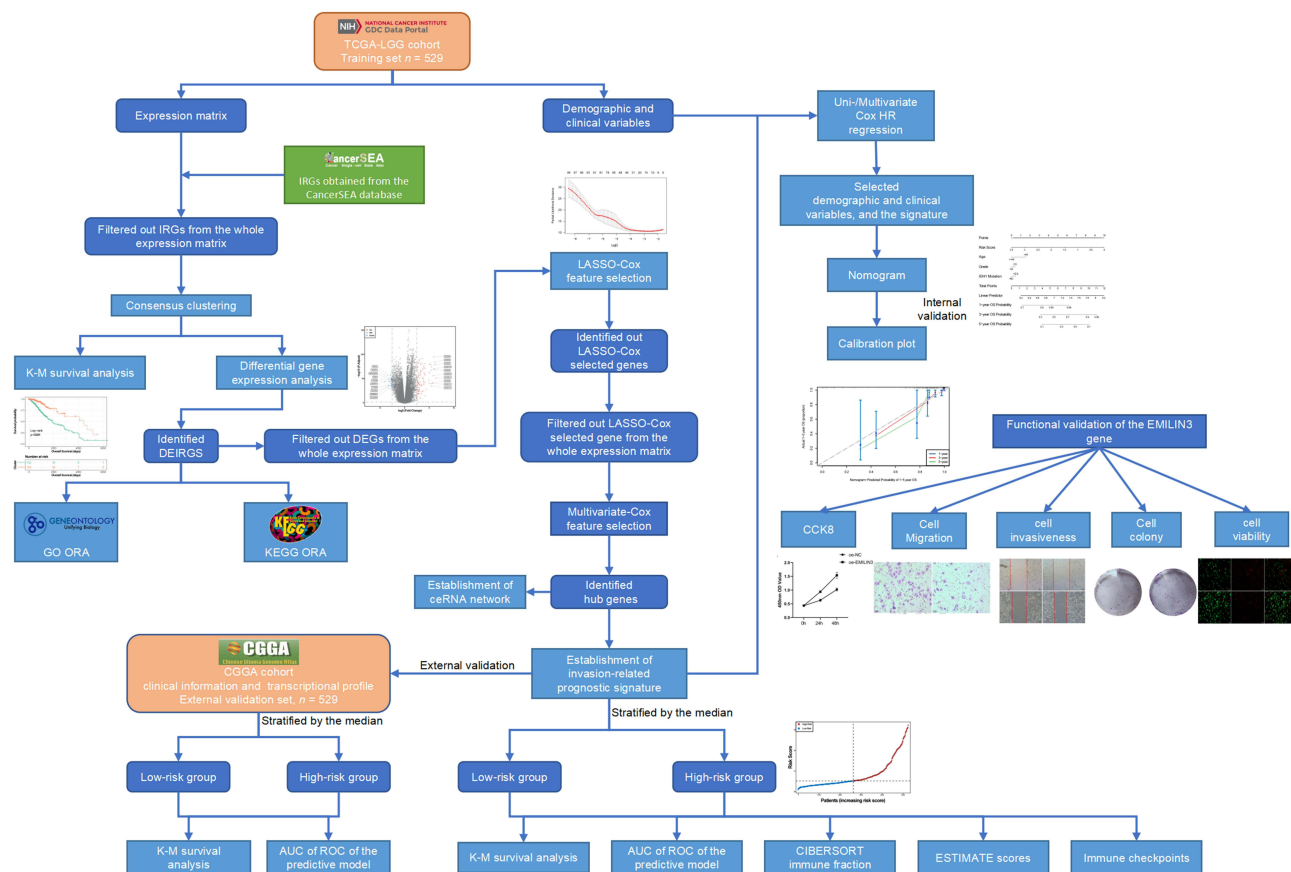


Figure 1 Study process map. This study involved the development of a low-grade glioma aggressiveness model by bioinformatics analysis of the TCGA and CGGA databases. After evaluating 10 markers associated with invasiveness in low-grade gliomas by various methods, we selected the EMILIN3 gene for further investigation. Our cell function experiments indicated that the EMILIN3 gene could potentially serve as a novel biological marker for invasiveness in low-grade gliomas.

Materials and Methods

Data Source

The training set included transcriptome and survival data from 529 LGG samples from the TCGA database (<https://portal.gdc.cancer.gov/>). Furthermore, an external validation set of 284 LGG samples was collected from the CGGA database (<http://www.cgga.org.cn/>). A total of 97 invasion-related genes (IRGs) were retrieved from the CancerSEA database (<http://bioacc.hrbmu.edu.cn/CancerSEA/>) ([Supplementary Table 1](#)).²³

Identification of DEGs Between Invasion-Related Molecular Subtypes

Based on 97 IRGs, we explored the potential invasion-related molecular subtypes of LGG samples in training set by consensus clustering using the “Consensus Cluster Plus” package (version 1.58.0).²⁴ Then, the survival analysis of invasion-related molecular clusters was performed using the R package “survival” (version 3.3.1).²⁵ The differentially expressed genes (DEGs) between the different invasion-related molecular subtypes of LGG were identified using the “DESeq2” R package (version 1.34.0)²⁶ with adj. $p < 0.05$ and $|\text{Log}_2\text{FC}| > 2.5$. The analysis findings were displayed using volcano plots and heatmaps created using the “ggplot2” (version 3.3.5) and “pheatmap” (version 1.0.12) R tools. The “clusterProfiler” (version 4.2.2) program was also used to perform Gene Ontology (GO) and Kyoto Encyclopedia of Genes and Genomes (KEGG) enrichment analyses for DEGs.²⁷

Establishment and Validation of the Risk Model

Based on the DEGs, the OS-related DEGs were identified using univariate Cox analysis ($\text{HR} \neq 1$, $P < 0.01$) and further filtered using the LASSO algorithm. This process yielded signature genes for constructing a risk model using the “glmnet” package (version 4.1.3). The risk model was generated using the formula: $\text{risk score} = \sum_{i=1}^n (\text{coef}_i * \text{Exp}_i)$, and LGG samples were divided into high- and low-risk groups based on the median risk score. Survival curves were plotted using the “survival” and “survminer” (version 0.4.9) packages. The model’s predictability was evaluated using ROC curves at 1-, 3-, and 5-year time points with the “survival ROC” R package (version 1.0.3). The validation set was used to verify the results. In addition, the risk scores were compared across various clinicopathological parameters, including Gender, Age, Grade, Isocitrate Dehydrogenase 1 (IDH1) gene mutation, and Histological Type.

Additionally, we analyzed the differences in the subgroup signature genes among various clinicopathological parameters. A p -value < 0.05 indicated a significant difference.

Nomogram Establishment

Based on the above-mentioned 6 clinicopathological parameters, this study applied univariate/multivariate Cox analyses and Proportional Hazards (PH) assumption test to sift independent predictors for constructing a nomogram (1-, 3-, and 5-year) to predict the OS. Then, the performance of it was evaluated by the calibration plot.

Tumor Immune Microenvironment and Immune Checkpoint Analyses

We applied the “ESTIMATE” package to calculate the immune score, ESTIMATE score, tumor purity, and stromal score and compared them between risk groups. Then, the CIBERSORT algorithm²⁸ was applied to detect immune cells in risk groups, and we compared the immune checkpoints’ expression between the risk groups ($p < 0.05$). Boxplot was generated to visualize the differences.

Regulation Network Construction

We predicted miRNAs and lncRNAs applying miRNet database²⁹ (<https://www.mirnet.ca>). Firstly, in training set, differentially expressed miRNA (DEmiRNA, $p < 0.05$ and $|\text{Log}_2\text{FC}| > 1$) and differentially expressed lncRNA (DElncRNA, adj. $p < 0.05$ and $|\text{Log}_2\text{FC}| > 0.5$) between the different invasion-related molecular subtypes of LGG samples were screened using the “DESeq2”. Then, miRNet database was employed to predict the miRNA targeting signature genes, and predict the lncRNAs targeting DEmiRNA. Then, DEmiRNA intersected with these predicted miRNAs to

procure the final miRNAs. DEIncRNA intersected with these predicted lncRNAs to procure final lncRNAs. Importantly, the ceRNA network was constructed eventually.

RNA Extraction and Validate the Hub Genes

According to the World Health Organization's classification of central nervous system tumours, gliomas may be classified as either low-grade (grades I–II) or high-grade. The isolation of total RNA was performed on a sample set consisting of 20 gliomas, including both 10 high-grade and 10 low-grade tumours. The Steady Pure Rapid RNA Extraction Kit (D7168M, Beyotime, China) was used for the experiment. The AG11706 Reverse Transcription Kit, manufactured in China, was used to perform reverse transcription on the extracted RNA samples. The cDNA was amplified using a SYBR premixed Ex Taq kit (AG11718, AG, China). The amplification of cDNA used 3-phosphoglyceraldehyde dehydrogenase as an internal reference. The assessment of mRNA expression was performed using the 2⁻(Delta CT) method. Table 1 lists all the primers in the study.

Reasons for Selecting the EMILIN3 Gene for Study

By searching the ten genes we pre-screened in PUBMED, we found that most of the genes are available in the literature in gliomas, but the literature of EMILIN3 gene in gliomas is less, so we chose this gene for the experimental validation.

In vitro Validation of the HUB Gene

Cell Culture and Cell Transfection

The LN229 and HS-683 human glioma cell line were purchased from iCell Bioscience Inc, and grown in DMEM media (Gibco, USA) with 10% foetal bovine serum (BI, USA) and 1g/mL penicillin/streptomycin (Hyclone, USA) at 37 degrees Celsius and 5% carbon dioxide. HASMC were transfected with a lentiviral expression vector containing the full-length EMILIN3 (Shanghai Genechem Co., Ltd, China) and the impact of transfection was measured using quantitative real-time polymerase chain reaction (qRT-PCR).

CCK-8 Detection of Cell Proliferation Capacity

Cells in the logarithmic growth phase were chosen and then digested using trypsin to create a cell suspension. The 1000 cells were put to 96-well plates, 10ul CCK-8 solution was added to each well at 0, 24, and 48h, incubated in the incubator for 0.5h, and enzyme markers were used to measure absorbance at 450 nm in each well.

Cell Viability Analysis

The cell viability of the LN-229 and HS-683 cell line in a high-fat media were evaluated using the Live/Dead Cell Kit manufactured by Biogradetech, a company based in China. Live cells were stained using calcein-AM, while dead cells were stained using propidium iodide. The fluorescence images were acquired using an OLYMPUS fluorescence microscope from Japan.

Table 1 Primers for RT-PCR

Gene	FORWARD Primer (5'-3')	Reverse Primer (5'-3')
<i>IGF2BP2</i>	AGCTAAGCGGGCATCAGTTTG	CCGCAGCGGGAAATCAATCT
<i>SRY</i>	AGAGAATCCCAGAATGCGAAAC	CTTCCGACGAGGTCGATACTT
<i>CHI3L1</i>	GTGAAGGCGTCTCAAACAGG	GAAGCGGTCAAGGGCATCT
<i>IGF2BP3</i>	ACGAAATATCCCGCCTCATTTAC	GCAGTTTCCGAGTCAGTGTTC
<i>MEOX2</i>	GGCAAGAGGAAAAGCGACAG	ATCTCGTATCGCCTCAGTCTG
<i>ABCC3</i>	CACCAACTCAGTCAAACGTGC	GCAAGACCATGAAAGCGACTC
<i>HOXC4</i>	GAGCGCCAGTATAGCTGCAC	GCGACTGTGATTTCTCGGGG
<i>OTP</i>	GCACAGCTCAACGAGTTGGA	GTCAGCCCCGATACGCAGTG
<i>METTL7B</i>	GCAACCGCAAGATGGAGAG	GATTTGGGTCTAGGCAGGTGA
<i>EMILIN3</i>	GGGGATGAGCTTACGAGGC	ATGTCCAACCTCAGACAGCAT

Cell Migration Capability in Wound-Healing Assay

Cells in the logarithmic growth phase that were in a healthy state were chosen. These cells were then treated with trypsin to break them down and transformed into a cell suspension. Following cell counting, the cells were introduced into sterile six-well plates with a density of 50,000 cells per well. Subsequently, the plates were placed in an incubator set at a temperature of 37°C and a CO₂ concentration of 5% for overnight incubation. Once the cells were evenly distributed across the well plates, perpendicular scratches were created on the bottom of the well plates using a sterile gun tip. The process of cell migration was captured using microscopic imaging at both the initial time point (0 hours) and after a 24-hour period. The Wound Healing Assay is used to assess the migratory ability of cells, as has been shown in earlier literature.³⁰

Transwell Assay for Cell Invasiveness

Transwell chambers were coated with 60 µL of 1 mg/mL matrigel (Corning, USA) to ensure equal distribution. Cells in the logarithmic growth phase that were in a healthy state were chosen. These cells were then digested using trypsin and transformed into a cell suspension using a medium that does not contain serum. After performing cell counting, a volume of 100 µL was extracted from a cell density of 5×10^5 cells/mL and evenly introduced into the lower chamber. Subsequently, the whole medium was added to the bottom chamber. The 24-well plate was then placed in an incubator set at a temperature of 37°C with a carbon dioxide concentration of 5% for a total incubation period of 72 hours. The cells were dyed with a 0.1% solution of crystal violet and examined using an inverted microscope.³¹

Clone Formation Experiments

The clonogenicity of LN-229 and HS-683 cells were tested using colony formation tests. 1500 uniformly dispersed cells were on six-well plates with medium changes for three days. A Biosharp (China) 4% paraformaldehyde solution fixed the cells after two weeks. The cells were stained with Solarbio (China) crystal violet. After three rounds of washing, the colonies were photographed.

Statistical Analysis

The biological experiments were analyzed using SPSS 25 software with at least three replications, and comparisons between the two groups were made using the independent samples *t*-test, with a *p*-value of less than 0.05 considered statistically significant.

Results

DEGs Identification Between Two Invasion-Related Molecular Subtypes

Two invasion-related molecular subtypes of LGG, cluster 1 and cluster 2, were identified at $k = 2$ (Figure 2A and B). A significant survival difference was detected between these two clusters, in which the patients in Cluster 1 had a poorer survival ($p < 0.0001$, Figure 2C). Then, we screened out 163 DEGs (Cluster 1 VS Cluster 2) (Figure 2D and E) to conduct Enrichment analyses. GO analysis identified that DEGs were involved in the “pattern specification process”, “regionalization”, “ion channel complex”, “transmembrane transporter complex”, etc (Figure 3A and B). As shown in Figure 3C and D, KEGG results contained “transcriptional misregulation in cancer” and “nicotine addiction.”

Risk Model Construction and Validation

Based on the 163 DEGs, Figure 4A indicated that 101 DEGs were significantly correlated with OS ($p < 0.01$). Then, we put the selected 101 genes into Lasso regression analysis, 10 signature genes were screened (Figure 4B and C). Risk scores were calculated as: Risk Score = 0.0885* expression (*IGF2BP2*) + 0.5225* expression (*SRY*) + 0.0369* expression (*CHI3L1*) + 0.1577* expression (*IGF2BP3*) + 0.0902* expression (*MEOX2*) + 0.07772* expression (*ABCC3*) + 0.0814* expression (*HOXC4*) + 0.0750* expression (*OTP*) + 0.1278* expression (*METTL7B*) + 0.0653* expression (*EMILIN3*). Based on the median risk score, samples were allocated into high-/low-risk groups. Their distribution and survival status implied that there were more dead with a risk score increase (Figure 4D and E), and we found that the high-risk group had a worse OS

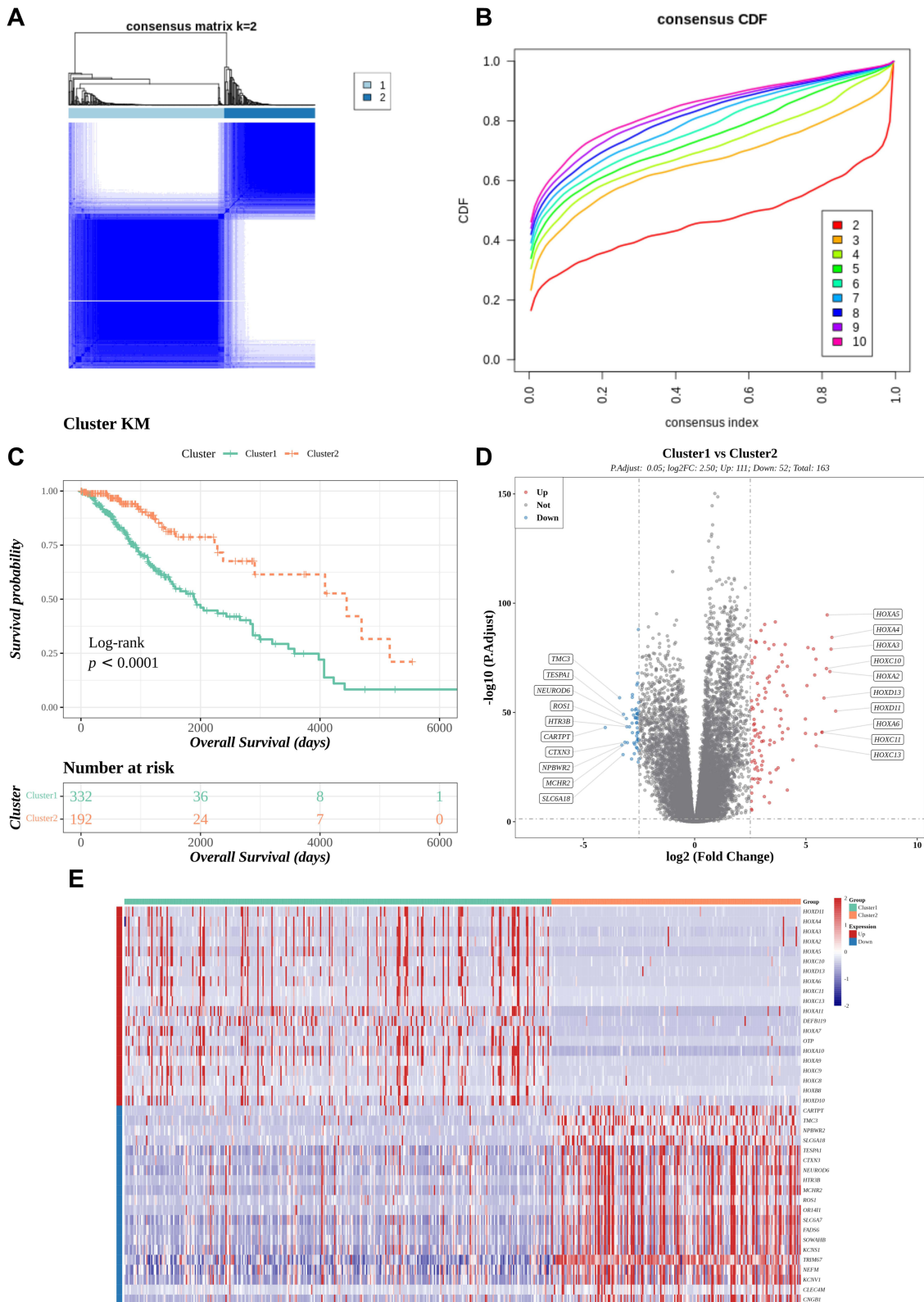


Figure 2 Cluster analysis based on invasion-related genes. (A and B) Cluster analysis revealed that the 529 LGG samples in the TCGA may be separated into two categories. (C) Survival analysis of clusters 1 and 2. (D) Volcanic map of differential genes between two clusters. (E) Heat map of differential genes.

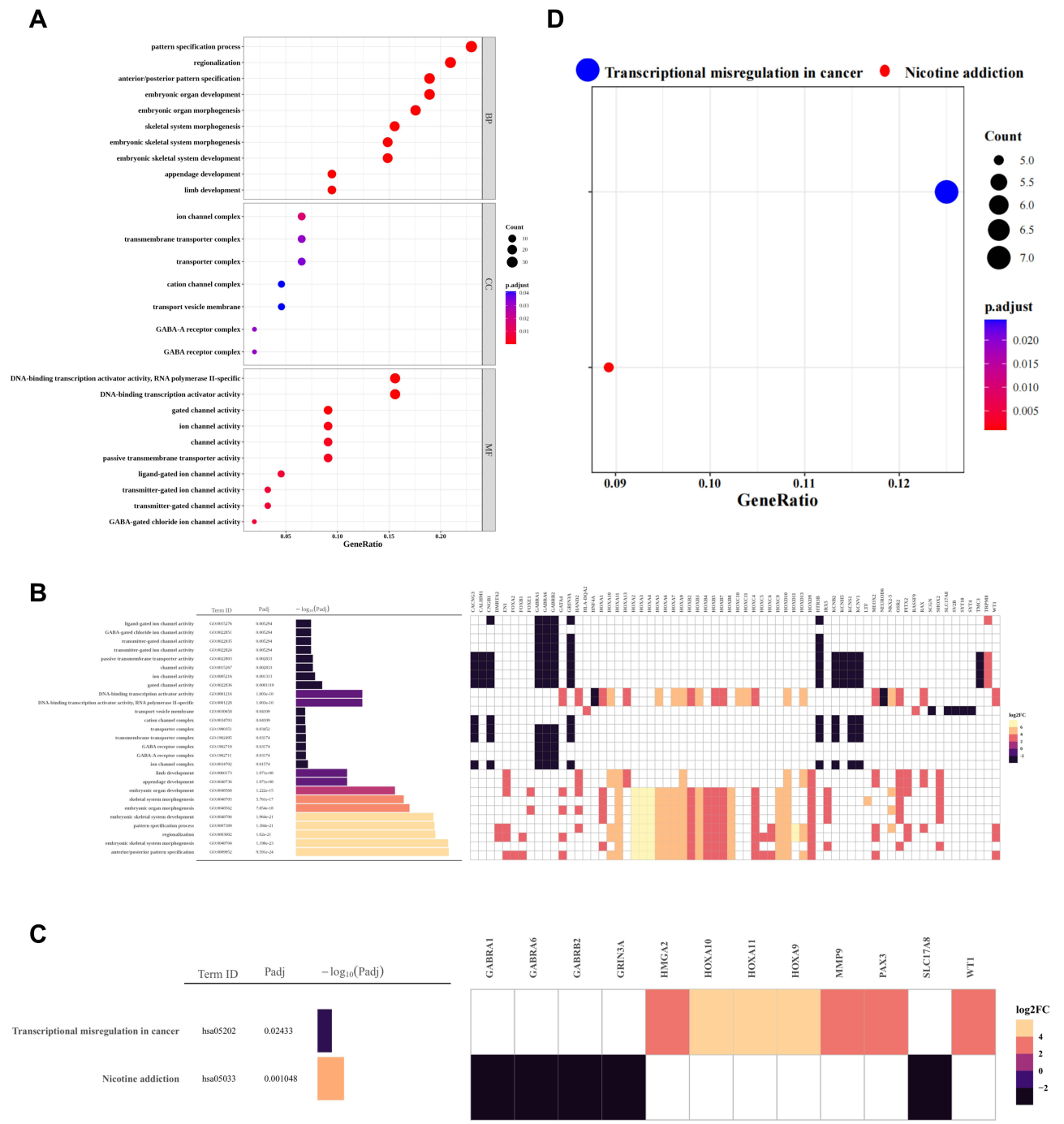


Figure 3 GO and KEGG. Significantly enriched GO terms and KEGG pathways of DEGs (adjusted $P < 0.05$). **(A-B)** Significantly enriched GO terms of DEGs. **(C-D)** Significantly enriched KEGG pathways of DEGs.

($p < 0.0001$) (Figure 4F). The AUC values determined by ROC curve analysis were 0.86, 0.86, and 0.78, suggesting a great outcome (Figure 4G). The samples in the validation set were examined using the same procedures as the training set, according to the formula developed by the TCGA cohort, and the findings were consistent (Figure 4H-K).

Nomogram Construction

Univariate analysis based on the training set showed that risk score, age, grade, IDH1 mutation, and histological type with survival correlations ($p < 0.05$) (Figure 5A). Then, we found that risk score, age, grade, and IDH1 mutation, were still

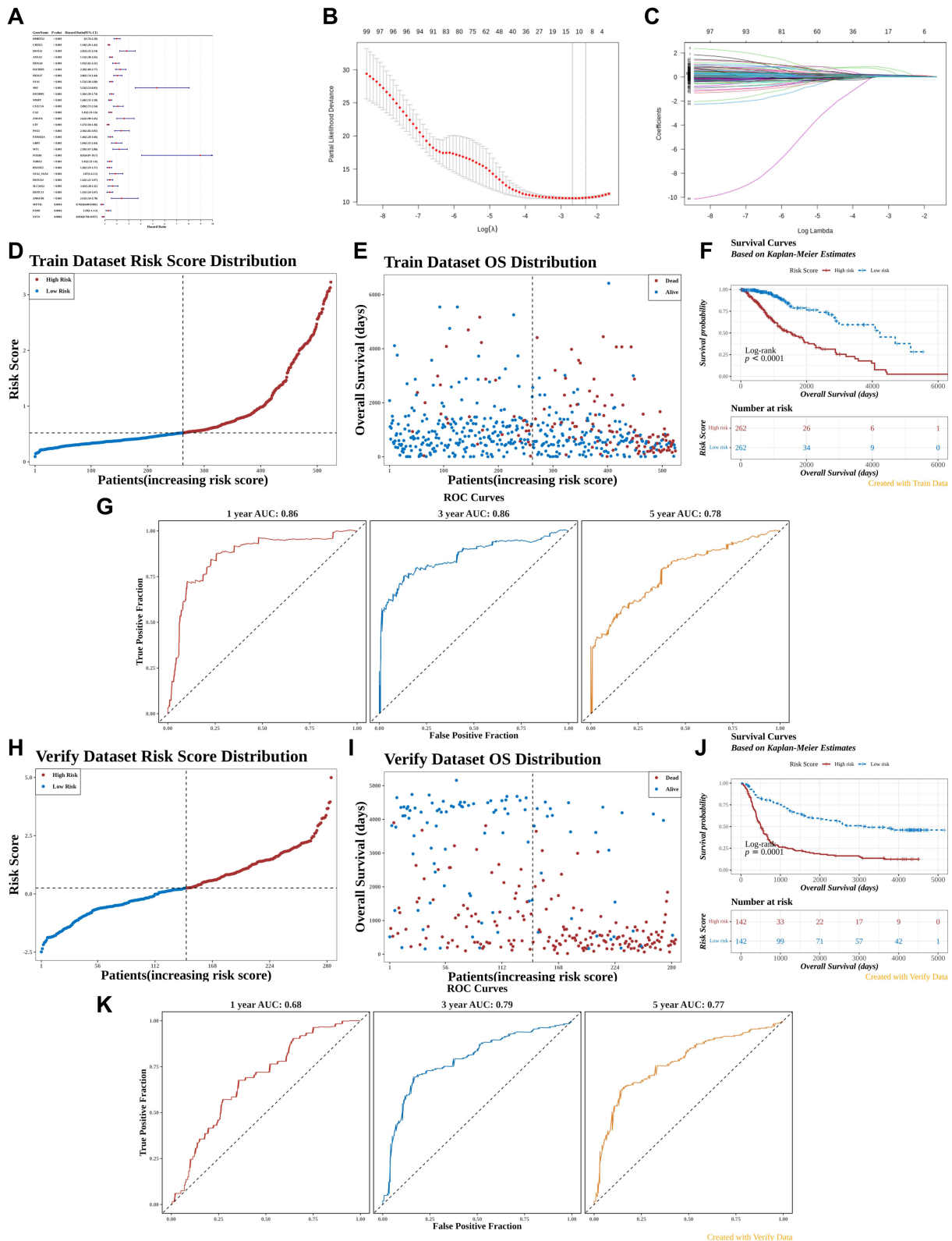
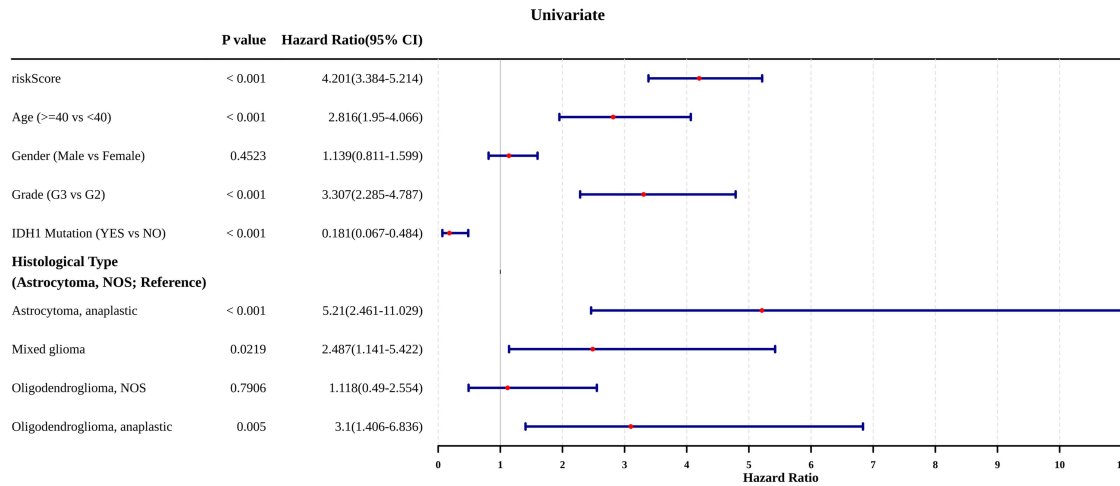
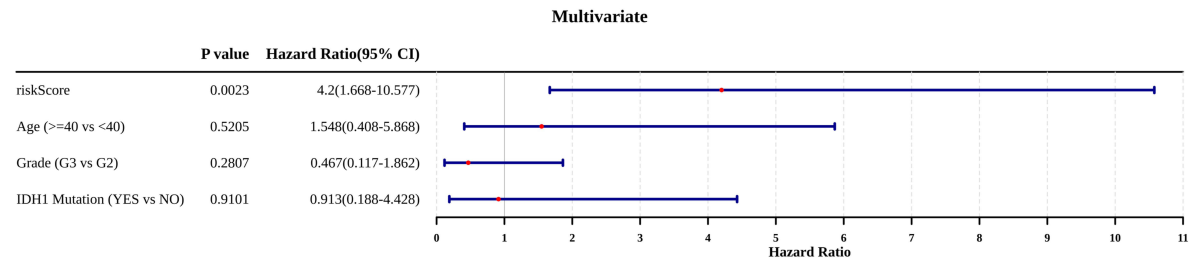


Figure 4 Building and validating the invasion-associated signature. (A) Univariable Cox regression. (B-C) Lasso regression analysis. (D) Distribution of patients' risk scores. (E) Survival times of patients plotted against their risk scores. (F) Overall survival (OS) differed significantly between the high-risk and low-risk groups. (G) The AUC curves of the signature for 1, 3, and 5 years in the TCGA cohort. (H-K) Validation of the invasion-related signature in the CGGA database.

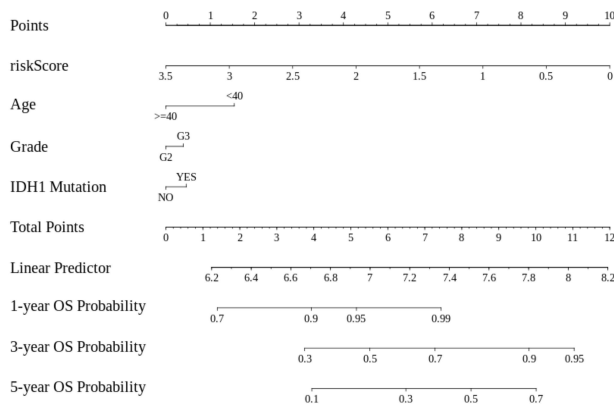
A



B



C



D

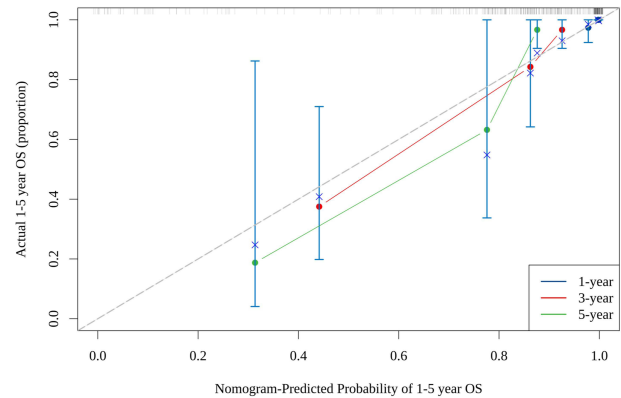


Figure 5 Evaluation of prognostic signature to predict the OS of LGG patients. **(A)** Univariate Cox regression. **(B)** Multivariate Cox regression. **(C)** In LGG patients, a nomogram was developed to predict 1-, 3-, and 5-year OS. **(D)** Calibration curves for the clinicopathologic invasion nomogram.

remarkably related to prognosis by multivariate Cox analysis (Figure 5B, Supplementary Table 2). As a result, we create the nomogram by combining the risk score, age, grade, and IDH1 mutation (Figure 5C), which is validated by the calibration curve (Figure 5D).

Risk Score in Different Clinicopathological Traits

In the present study, results of the Wilcoxon test demonstrated that risk scores were significantly different in age (<40, >40), grade (G2, G3), and IDH1 mutation (YES, NO) (Figure 6A-C). Kruskal–Wallis test demonstrated that risk scores

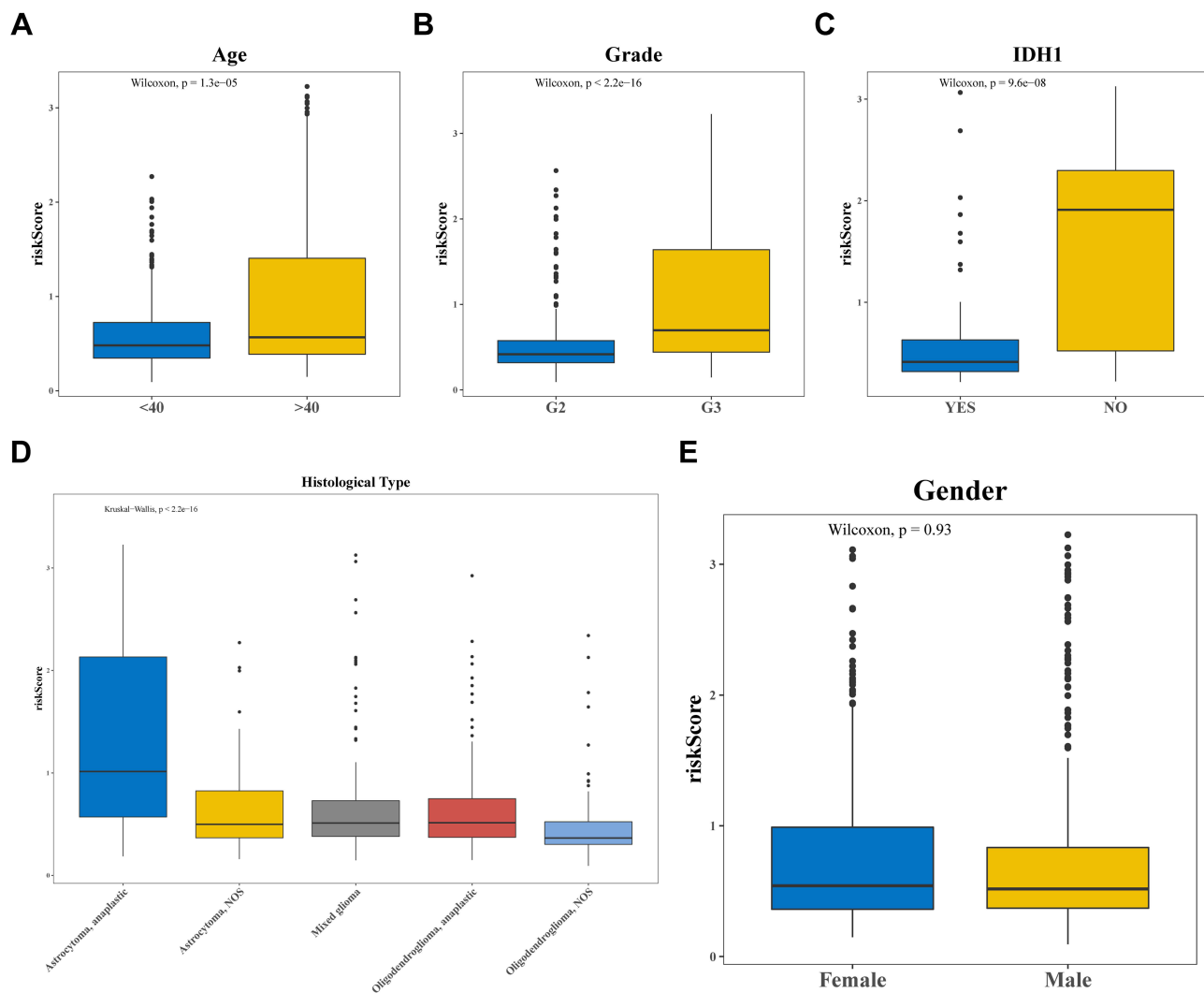


Figure 6 Evaluation of the risk model and clinical indicators in LGG patients. Comparison of the risk score in TCGA-LGG patients with varying degrees of various clinical factors (A) Age (B) Grade (C) IDH1 mutation (D) histological type (E) Gender.

are significantly different in histological types (anaplastic, astrocytoma, mixed glioma, NOS, oligodendroglioma, astrocytoma, anaplastic, and oligodendroglioma) (Figure 6D). Wilcoxon test demonstrated that the risk score was not significantly different between gender (female, male) (Figure 6E).

Furthermore, *ABCC3*, *CHI3L1*, *IGF2BP3*, *MEOX2*, *METTL7B*, and *OTP* showed significantly higher expression in the age > 40 subgroups (Figure 7A). Most of the significant genes exhibited significantly high expression in the G3 subgroups of Grade, except for *MEOX2* and *SRY* (Figure 7B). Similarly, most of the significant genes showed significantly high expression in the YES subgroups of IDH1 mutation, except for *EMILIN3* and *MEOX2* (Figure 7C). Only *SRY* had significantly higher expression in the male subgroups of Gender (Figure 7D).

Tumor Immune Microenvironment and Immune Checkpoint Analyses

Figure 8A demonstrates that the high-risk group exhibited elevated immune, stromal, and ESTIMATE scores based on our data. Significant differences in 13 cell types were observed between the risk groups, as shown in Figure 8B and C. Additionally, we observed higher expression of immune checkpoints (*ADORA2A* and *CD200*) in the low-risk group, while the high-risk group displayed increased expression of *BTLA*, *CD160*, *CD200R1*, *CD244*, and *CD27*, as depicted in Supplementary Table 3 and Figure 8D.

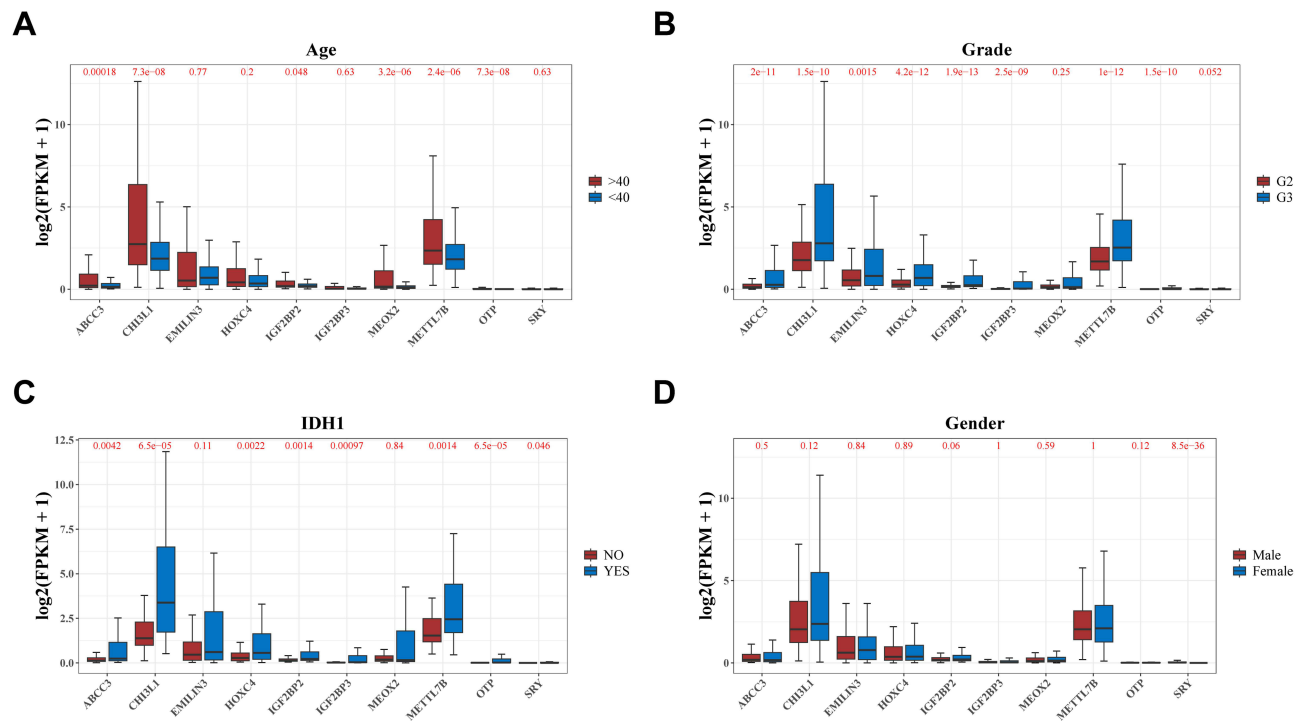


Figure 7 Evaluation of the prognostic signature genes and clinical indicators in LGG patients. Comparison of the expression of 10 signature genes in different clinic factor subgroups (A) Age (B) Grade (C) IDH1 mutation (D) Gender.

Construction of ceRNA Regulatory Network

In brief, the DESeq2 package tested 29 DEMiRNAs and 2411 DELncRNAs. Five miRNAs intersected two hundred two miRNAs predicted by model genes and 29 DEMiRNAs. Then we found 228 DEMiRNA lncRNAs. By taking the intersection of 228 lncRNAs and 2411 DELncRNAs, 11 lncRNAs were found. Finally, a ceRNA network of three lncRNAs, three miRNAs, and five mRNAs was built (Figure 9).

Screening and in vivo Validation of Model Genes

The quantitative real-time polymerase chain reaction (qRT-PCR) findings indicate that the expression levels of *HOXC4* (Figure 10A), *ABCC3* (Figure 10B), *EMILIN3* (Figure 10C), *CHI3L1* (Figure 10D), *IGF2BP3* (Figure 10E), *MEOX2* (Figure 10F), *IGF2BP2* (Figure 10G), *OTP* (Figure 10H), *METTL7B* (Figure 10I), and *SRY* (Figure 10J) were considerably higher in high-grade gliomas compared to low-grade gliomas.

EMILIN3 Gene Function Experiment

The qRT-PCR indicated LN229 and HS-683 human glioma cells transfected well (Figures 11A and 12A). Live/dead staining and cck8 test demonstrated that overexpression of *EMILIN3* gene improved LN229 and HS-683 cell line proliferation and viability (Figure 11B, C, 12B and C); viability of LN229 and HS-683 cell line (Figures 11C and 12C); cell scratch assay suggested that overexpression of *EMILIN3* gene could improve migration (Figures 11D and 12D); transwell results suggested that overexpression could improve invasion (Figures 11E and 12E); and colony formation assay suggested that could improve colony formation (Figures 11F and 12F).

Discussion

LGG is a widely known aggressive, primary intracranial tumor, and the prognosis of patients remains bleak even after they have undergone optimal clinical interventions such as surgical resection, radiotherapy, and chemotherapy to ensure maximum safety.³² The leading cause of this poor prognosis is the diffuse, aggressive growth of glioma cells, which not only prevents complete surgical tumor removal but also promotes resistance of the tumor tissue to chemotherapy and

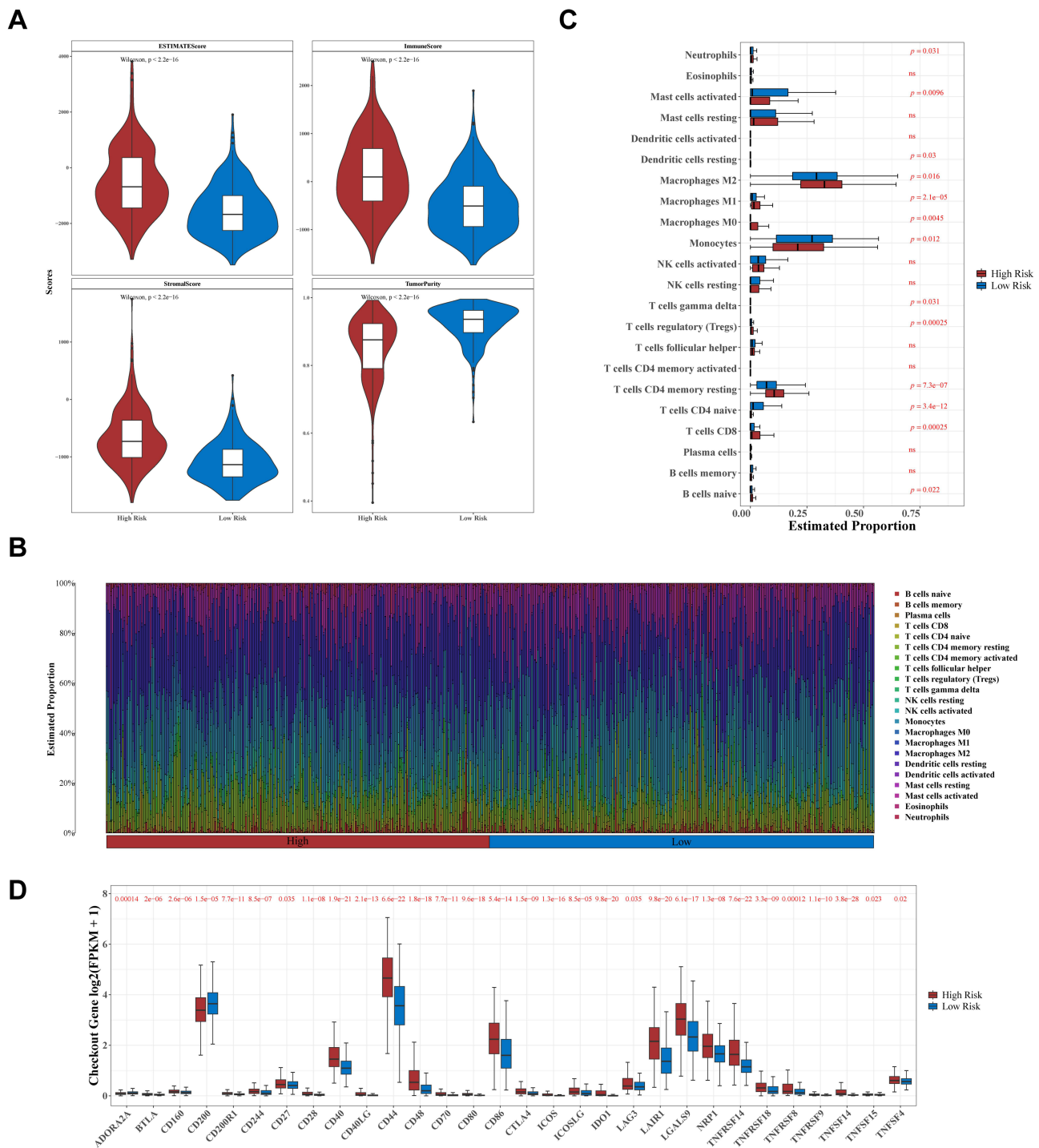


Figure 8 The two groups' tumor-immune microenvironments were examined. **(A)** In two groups, ESTIMATE score, immune score, stromal score, and tumor purity were calculated. **(B)** The percentage of immunological cells. **(C)** Comparison of tumor-infiltrating immune cells in two groups. **(D)** Comparison of immunological checkpoints in two groups.

radiotherapy.³³ The invasion has a crucial role in the development of LGG. Although there have been many in vitro and in vivo studies on LGG, some mechanisms are unknown due to the complexity of its invasive system.³³ Therefore, exploring new targets will provide new insights into the exploration of LGG therapy and its molecular mechanisms.

In LGG, we found two invasion-related molecular subtypes, cluster 1 and cluster 2. Cluster 2 had a worse prognosis. In an enrichment analysis of the differentially expressed genes between these subtypes, we found significant enrichments

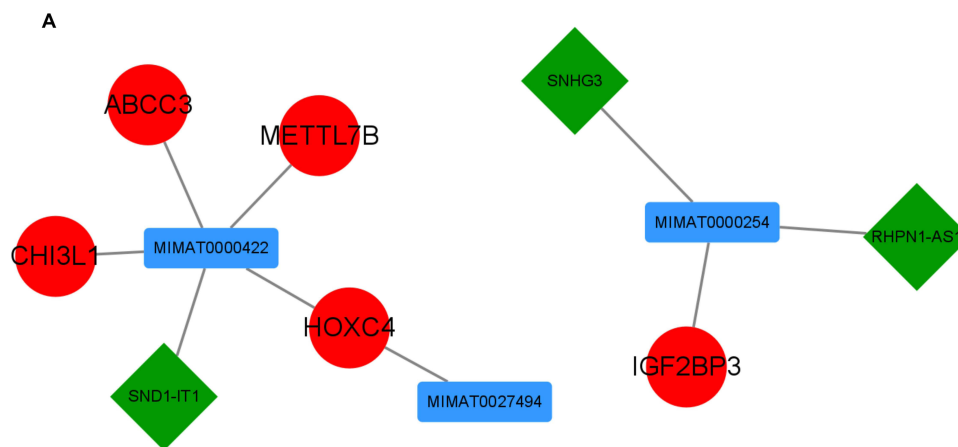


Figure 9 Construction of ceRNA regulatory network with model genes.

in GABA-related processes like GABA and GABA-A receptor complexes, GABA-gated chloride channel activity, RNA polymerase II specificity, and nicotine addiction-related entries. GABA, a non-protein amino acid, is a key central nervous system inhibitor. Animals, plants, and microbes naturally contain it.³⁴ Astrocytes facilitate neuronal function by breaking down glutamate and GABA. GABA transaminase and succinate semialdehyde dehydrogenase (*SSADH*) convert GABA into succinate, which contributes to the TCA cycle.³⁵ Isocitrate dehydrogenase (*IDH*) mutations cause glioma cells to adaptively drive the TCA cycle, promoting tumour growth. *IDH* mutations are common in LGG.^{36,37} RNA polymerase II (Pol II) is essential for eukaryotic cell protein-coding gene transcription.³⁸ In gliomas, abnormal expression of the long non-coding RNA HOTAIR greatly affects malignancy. Its abnormal activation is linked to immunological response, T cells, and Pol II.³⁹ Nicotine increases *CYP2B1* expression in glioma tissues, particularly the cerebral cortex and blood vessels.⁴⁰

We used univariate regression with lasso regression to find eleven characteristic genes that affect glioma. Risk models were created using these genes and displayed in column line graphs. *IGF2BP2*, an *IGF2* mRNA-binding protein, regulates mRNA localization, stability, and translation.^{41,42} High-grade gliomas are thought to be more malignant and have a worse prognosis. To further validate the role of these 10 model genes in gliomas, we selected 10 high-grade and 10 low-grade cases for qRT-PCR validation. The high level of expression in high-grade gliomas indirectly suggests that these model genes are detrimental to glioma prognosis and have some predictive potential. Pancreatic cancer tumour cell proliferation is increased by *IGF2BP2* overexpression via the PI3K/Akt signalling pathway.⁴³ FBXL19-AS1 and tight junction-related protein expression is considerably reduced by nervous system *IGF2BP2* knockdown, increasing blood-tumor barrier permeability and decreasing *ZNF765* expression through STAU1-mediated mRNA decay.⁴⁴ LI et al found that *IGF2BP2* binds to *SUMO1* and regulates the OIP5-AS1/miR-495-3p axis, increasing glioma angiogenesis. Sex-determining region-Y (*SRY*) genes in the *SOX* family generate the male phenotype, which female mammals do not express.^{45,46} *SOX-2* protein expression promotes cell invasion in neural and neural crest-origin tumours, including gliomas.⁴⁷ *SOX-2* enhances cancer cell differentiation, and inhibiting it in glioblastoma-implanted cells lowers tumorigenicity and proliferation in immunodeficient animals.^{48,49} Cancers include breast, colorectal, ovarian, prostate, lung, and glioblastoma have higher serum levels of *CHI3L1* (YKL-40), a secreted glycoprotein.^{50,51} High serum *CHI3L1* levels predict glioma grading and poor prognosis.^{52–56} RNA-binding protein *IGF2BP3* is mostly detected in foetal tissues and seldom in adult tissues. Cancers with high *IGF2BP3* expression, particularly gliomas, have poor prognoses.⁵⁷ *MEOX2*, a homologous box transcription factor, is essential for tissue development. Its overexpression causes cell cycle arrest and endothelial cell senescence and is linked to poor glioma prognosis.^{58–61} *ABCC3*, a member of the ATP-binding cassette (ABC) protein superfamily, can cause brain drug resistance, especially to cytotoxic and antiviral medicines.⁶² By affecting eukaryotic transcription factors, *HOXC4* affects plant and animal development.⁶³ Overexpression of *HOXC4* and other *HOX* genes is linked to poor survival in radiation and chemotherapy-treated glioma patients.^{64–66} *METTL7B*, a methyltransferase-like protein, is abundantly expressed in papillary thyroid carcinoma and

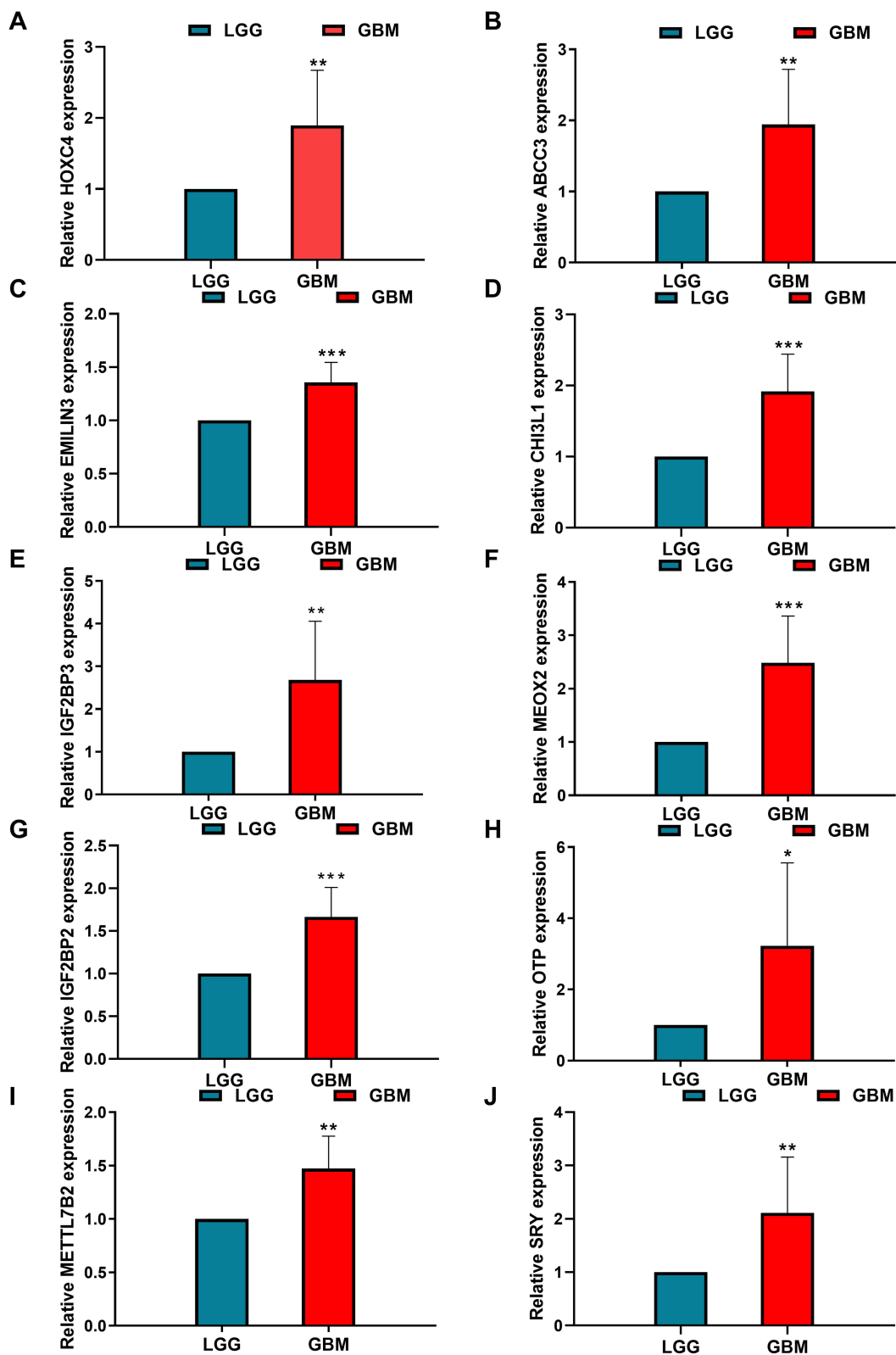


Figure 10 PCR validation of clinical glioma samples. The quantitative real-time polymerase chain reaction (qRT-PCR) findings indicate that the expression levels of HOXC4 (A), ABCC3 (B), EMILIN3 (C), CHI3L1 (D), IGF2BP3 (E), MEOX2 (F), IGF2BP2 (G), OTP (H), METTL7B (I), and SRY (J) were significantly elevated in high-grade gliomas compared to low-grade gliomas.

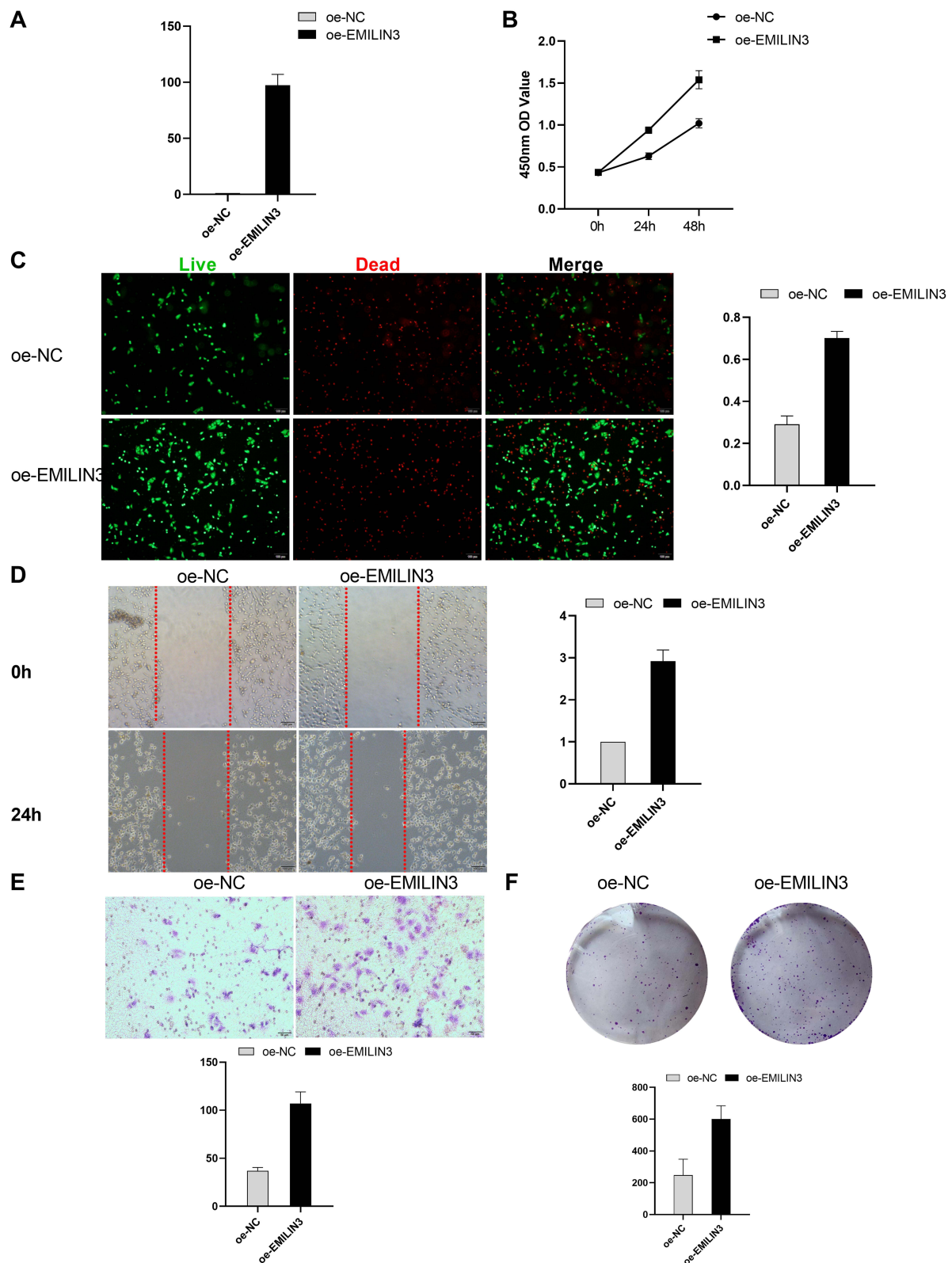


Figure 11 EMILIN3 gene function experiment in LN229. qRT-PCR transfected LN229 human glioma cells efficiently (**A**). The CCK-8 experiment and live/dead staining findings demonstrated that overexpression of the *EMILIN3* gene may increase LN229 cell line proliferation and vitality (**B** and **C**). Overexpression of the *EMILIN3* gene enhances the migration, invasiveness, and colony formation of the LN229 cell line (**D-F**).

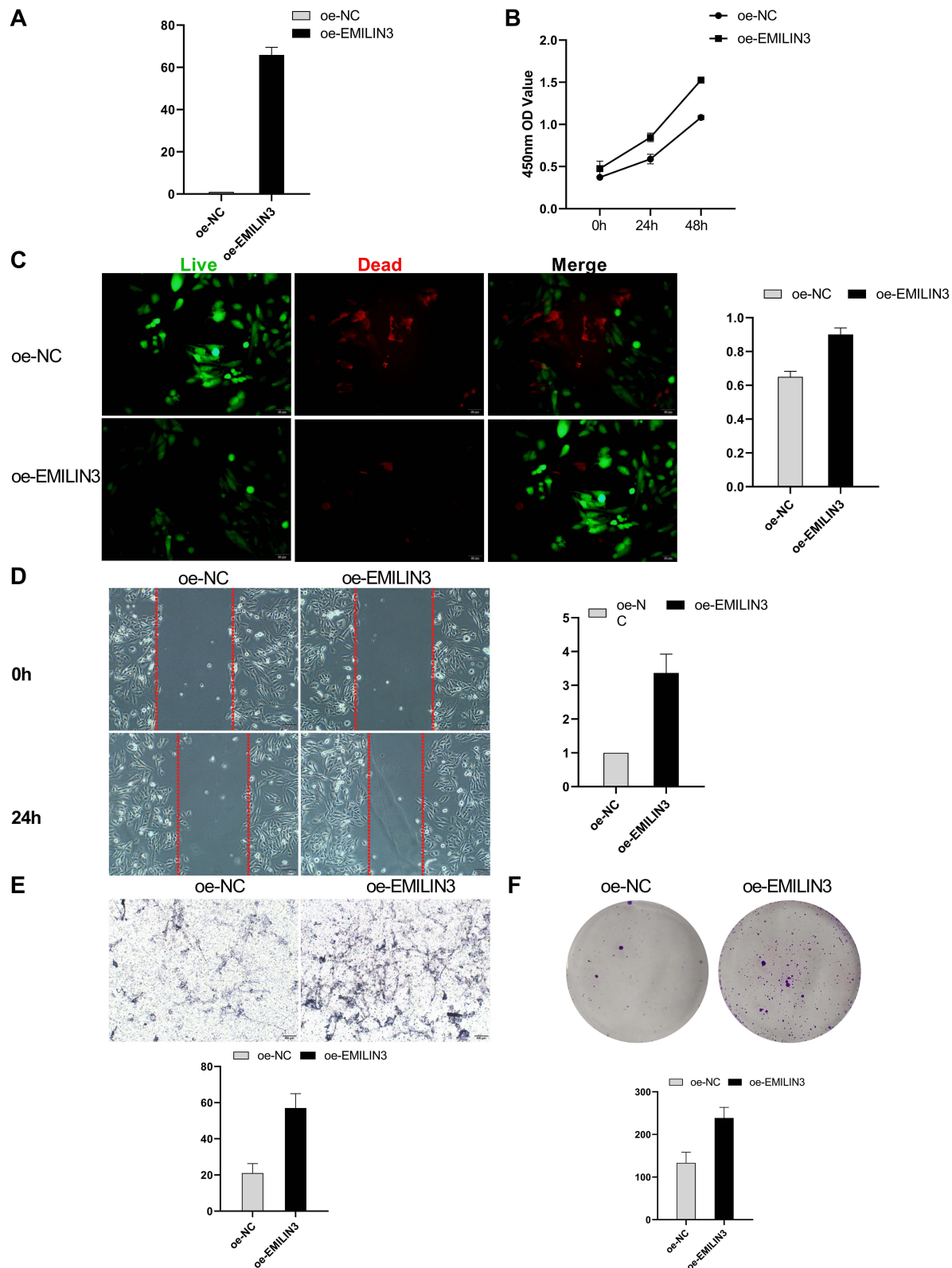


Figure 12 EMILIN3 gene function experiment in HS-683. qRT-PCR transfected HS-683 human glioma cells efficiently (A). The CCK-8 experiment and live/dead staining findings demonstrated that overexpression of the *EMILIN3* gene may increase HS-683 cell line proliferation and vitality (B and C). Overexpression of the *EMILIN3* gene enhances the migration, invasiveness, and colony formation of the HS-683 cell line (D-F).

enhances thyroid cancer cell motility and invasion.^{67,68} High *METTL7B* expression in gliomas promotes LGG progression and death.⁶⁹ *EMILIN3*, a glycoprotein in the extracellular matrix, controls TGF- β ligand activity.⁷⁰ Heparin and heparan sulphate proteoglycans contribute to glioma formation, which worsens high-risk LGG prognosis.^{71,72} *EMILIN3*'s significance in gliomas is unclear, hence more research was done in in vitro cells. In the LN229 and HS-683 human glioma cell line, *EMILIN3* stimulated cell viability, proliferation, migration, invasiveness, and colony formation. Signature genes contribute to LGG and related illnesses in many ways. They have theoretical validity and diverse uses as patient prognostic markers.

In LGG, cancer cells utilize self-regulation mechanisms to evade immune cells, promoting immune escape and facilitating tumor progression. Immune checkpoint inhibitors (ICIs) have gained significant interest for their potential to target negative immunomodulatory factors like CTLA-4, PD-1, and PD-L1.⁷³ Our study revealed notable differences in the expression levels of approximately 30 immune checkpoints between the high and low-risk groups. Notably, *BLTA* and *CD160*, which share the same ligand, inhibit T-cell function and signaling through phosphorylation and recruitment of *SHP1* or *SHP2*.^{74,75} CTLA-4, which exhibits higher binding affinity to CD80 and CD86 than CD28, can diminish CD28 signaling by reducing CD80 and CD86 expression on antigen-presenting cells through trans endocytosis when expressed on T cells.^{76,77} Ongoing clinical Phase I/II studies for glioma immunotherapy involve CD27 inhibitor V sarilumab (CDX-1127), CTLA-4 inhibitors Ipilimumab (MDX-010, MDX-101), and Tremelimumab (ticilimumab, CP-675206).⁷⁸ Furthermore, we screened for three miRNAs that regulate signature genes and three long non-coding RNAs (lncRNAs) that control these miRNAs. sND1-IT1 has been implicated in various human diseases, including myocardial ischemia/reperfusion injury and laryngeal squamous cell carcinoma.⁷⁹ Studies have demonstrated its role in promoting TGF- β 1-induced epithelial-to-mesenchymal transition in gastric cancer through the miR-124/COL4A1 regulatory axis.⁸⁰ SNHG3, a well-known oncogenic lncRNA, is significantly upregulated in gliomas, promoting cell proliferation, inhibiting apoptosis, and influencing the cell cycle, thereby facilitating cancer progression.⁸¹

Conclusion

Ten invasion-associated signature genes were identified, and a risk model and line graph were developed to predict glioma patients' prognosis accurately. We performed PCR on clinical tumor samples for all ten genes, and the results were consistent with the predicted trends. We selected the *EMILIN3* gene for functional validation and found that this is a new gene that promotes aggressive transformation in gliomas.

Data Sharing Statement

The datasets used in this study can be accessed from the TCGA count (<https://portal.gdc.cancer.gov>) and the CGGA database (<http://www.cgga.org.cn/>). The invasion-related genes were obtained from the CancerSEA database (<http://bioacc.hrbmu.edu.cn/CancerSEA/>). For further details, please refer to the "Availability of data" section in the Materials and Data Policies of the Author's Guide.

Ethics Statement

Ethical permission for the current investigation was obtained from the Ethics Committee of Liaocheng People's Hospital (permission No. 2023015). The patients/participants provided their written informed consent to participate in this study. The present study fulfils the requirements of the Declaration of Helsinki.

Funding

Qilu Sanitation and Health Leading Talent Cultivation Project (to Zhiming Zheng, 2020-2025).

Disclosure

The authors declare that there is no conflicts of interest.

References

1. Mafi A, Rahmati A, Babaei Aghdam Z, et al. Recent insights into the microRNA-dependent modulation of gliomas from pathogenesis to diagnosis and treatment. *Cell. Mol. Biol. Lett.* 2022;27(1):65.
2. Lin D, Wang M, Chen Y, et al. Trends in Intracranial Glioma Incidence and Mortality in the United States, 1975-2018. *Front Oncol.* 2021;11:748061.
3. Thakkar JP, Dolecek TA, Horbinski C, et al. Epidemiologic and molecular prognostic review of glioblastoma. *Cancer Epidemiol Biomarkers Prev.* 2014;23(10):1985–1996.
4. Schiff D, Van den Bent M, Vogelbaum MA, et al. Recent developments and future directions in adult lower-grade gliomas: society for Neuro-Oncology (SNO) and European Association of Neuro-Oncology (EANO) consensus. *Neuro-Oncology.* 2019;21(7):837–853.
5. Weller M, van den Bent M, Tonn JC, et al. European Association for Neuro-Oncology (EANO) guideline on the diagnosis and treatment of adult astrocytic and oligodendroglial gliomas. *Lancet Oncol.* 2017;18(6):e315–e29.
6. Ater JL, Zhou T, Holmes E, et al. Randomized study of two chemotherapy regimens for treatment of low-grade glioma in young children: a report from the Children's Oncology Group. *J Clin Oncol.* 2012;30(21):2641–2647.
7. Kiran M, Chatrath A, Tang X, Keenan DM, Dutta A. A Prognostic Signature for Lower Grade Gliomas Based on Expression of Long Non-Coding RNAs. *Mol Neurobiol.* 2019;56(7):4786–4798.
8. Burger PC, Heinz ER, Shibata T, Kleihues P. Topographic anatomy and CT correlations in the untreated glioblastoma multiforme. *J Neurosurg.* 1988;68(5):698–704.
9. Cuddapah VA, Robel S, Watkins S, Sontheimer H. A neurocentric perspective on glioma invasion. *Nat Rev Neurosci.* 2014;15(7):455–465.
10. Guo X, Jiao H, Cao L, Meng F. Biological implications and clinical potential of invasion and migration related miRNAs in glioma. *Front Integrative Neurosci.* 2022;16:989029.
11. Chen W, Huang B, Wang E, Wang X. MiR-145 inhibits EGF-induced epithelial-to-mesenchymal transition via targeting Smad2 in human glioblastoma. *Oncotargets Ther.* 2019;12:3099–3107.
12. Wang Q, Li X, Zhu Y, Yang P. MicroRNA-16 suppresses epithelial-mesenchymal transition-related gene expression in human glioma. *Mol Med Rep.* 2014;10(6):3310–3314.
13. Valtorta S, Salvatore D, Rainone P, Belloli S, Bertoli G, Moresco RM. Molecular and Cellular Complexity of Glioma. Focus on Tumour Microenvironment and the Use of Molecular and Imaging Biomarkers to Overcome Treatment Resistance. *Int J Mol Sci.* 2020;21(16):67.
14. Pientka FK, Hu J, Schindler SG, et al. Oxygen sensing by the prolyl-4-hydroxylase PHD2 within the nuclear compartment and the influence of compartmentalisation on HIF-1 signalling. *J Cell Sci.* 2012;125(Pt 21):5168–5176.
15. Dai D, Huang W, Lu Q, Chen H, Liu J, Hong B. miR-24 regulates angiogenesis in gliomas. *Mol Med Rep.* 2018;18(1):358–368.
16. Liu S, Yin F, Zhang J, et al. Regulatory roles of miRNA in the human neural stem cell transformation to glioma stem cells. *J Cell Biochem.* 2014;115(8):1368–1380.
17. Qian BZ, Pollard JW. Macrophage diversity enhances tumor progression and metastasis. *Cell.* 2010;141(1):39–51.
18. Hambardzumyan D, Gutmann DH, Kettenmann H. The role of microglia and macrophages in glioma maintenance and progression. *Nat Neurosci.* 2016;19(1):20–27.
19. Gatenby RA, Gawlinski ET. The glycolytic phenotype in carcinogenesis and tumor invasion: insights through mathematical models. *Cancer Res.* 2003;63(14):3847–3854.
20. Bansal R, Magge S, Winkler S. Specific inhibitor of FGF receptor signaling: FGF-2-mediated effects on proliferation, differentiation, and MAPK activation are inhibited by PD173074 in oligodendrocyte-lineage cells. *J Neurosci Res.* 2003;74(4):486–493.
21. Wu M, Li X, Liu R, Yuan H, Liu W, Liu Z. Development and validation of a metastasis-related Gene Signature for predicting the Overall Survival in patients with Pancreatic Ductal Adenocarcinoma. *J Cancer.* 2020;11(21):6299–6318.
22. Liu J, Jiang C, Xu C, et al. Identification and development of a novel invasion-related gene signature for prognosis prediction in colon adenocarcinoma. *Can Cell Inter.* 2021;21(1):101.
23. Naba A, Clauser KR, Ding H, Whittaker CA, Carr SA, Hynes RO. The extracellular matrix: tools and insights for the “omics” era. *Matrix Biol.* 2016;49:10–24.
24. Wilkerson MD, Hayes DN. ConsensusClusterPlus: a class discovery tool with confidence assessments and item tracking. *Bioinformatics.* 2010;26(12):1572–1573.
25. Lei C, Chen W, Wang Y, et al. Prognostic Prediction Model for Glioblastoma: a Metabolic Gene Signature and Independent External Validation. *J Cancer.* 2021;12(13):3796–3808.
26. Love MI, Huber W, Anders S. Moderated estimation of fold change and dispersion for RNA-seq data with DESeq2. *Genome Biol.* 2014;15(12):550.
27. Yu G, Wang LG, Han Y, He QY. clusterProfiler: an R package for comparing biological themes among gene clusters. *OmicS.* 2012;16(5):284–287.
28. Chen B, Khodadoust MS, Liu CL, Newman AM, Alizadeh AA. Profiling Tumor Infiltrating Immune Cells with CIBERSORT. *Methods Mol Biol.* 2018;1711:243–259.
29. Fan Y, Xia J. miRNet-Functional Analysis and Visual Exploration of miRNA-Target Interactions in a Network Context. *Methods Mol Biol.* 2018;1819:215–233.
30. Grada A, Otero-Vinas M, Prieto-Castrillo F, Obagi Z, Falanga V. Research Techniques Made Simple: analysis of Collective Cell Migration Using the Wound Healing Assay. *J Investigative Dermatol.* 2017;137(2):e11–e6.
31. Wu D, Kang L, Tian J, et al. Exosomes Derived from Bone Mesenchymal Stem Cells with the Stimulation of Fe(3)O(4) Nanoparticles and Static Magnetic Field Enhance Wound Healing Through Upregulated miR-21-5p. *Int j Nanomed.* 2020;15:7979–7993.
32. de Gooijer MC, Guillén Navarro M, Bernards R, Wurdinger T, van Tellingen O. An Experimenter's Guide to Glioblastoma Invasion Pathways. *Trends Mol Med.* 2018;24(9):763–780.
33. Nakada M, Kita D, Teng L, et al. Receptor Tyrosine Kinases: principles and Functions in Glioma Invasion. *Adv Exp Med Biol.* 2020;1202:151–178.
34. Krnjević K, Schwartz S. Is gamma-aminobutyric acid an inhibitory transmitter? *Nature.* 1966;211(5056):1372–1374.
35. Schousboe A, Bak LK, Waagepetersen HS. Astrocytic Control of Biosynthesis and Turnover of the Neurotransmitters Glutamate and GABA. *Front Endocrinol.* 2013;4:102.

36. Sciacovelli M, Gonçalves E, Johnson TI, et al. Fumarate is an epigenetic modifier that elicits epithelial-to-mesenchymal transition. *Nature*. 2016;537(7621):r67.
37. Hujber Z, Horváth G, Petővári G, et al. GABA, glutamine, glutamate oxidation and succinic semialdehyde dehydrogenase expression in human gliomas. *J Exp Clin Cancer Res*. 2018;37(1):271.
38. Roeder RG, Rutter WJ. Multiple forms of DNA-dependent RNA polymerase in eukaryotic organisms. *Nature*. 1969;224(5216):234–237.
39. Wang Y, Yi K, Liu X, et al. HOTAIR Up-Regulation Activates NF- κ B to Induce Immunescape in Gliomas. *Front Immunol*. 2021;12:785463.
40. Nava-Salazar S, Gómez-Manzo S, Marcial-Quino J, et al. Effect of Nicotine on CYP2B1 Expression in a Glioma Animal Model and Analysis of CYP2B6 Expression in Pediatric Gliomas. *Int J Mol Sci*. 2018;19(6).
41. Bell JL, Wächter K, Mühleck B, et al. Insulin-like growth factor 2 mRNA-binding proteins (IGF2BPs): post-transcriptional drivers of cancer progression? Cellular and molecular life sciences. *CMLS*. 2013;70(15):2657–2675.
42. Christiansen J, Kolte AM, Hansen T, Nielsen FC. IGF2 mRNA-binding protein 2: biological function and putative role in type 2 diabetes. *J Mol Endocrinol*. 2009;43(5):187–195.
43. Xu X, Yu Y, Zong K, Lv P, Gu Y. Up-regulation of IGF2BP2 by multiple mechanisms in pancreatic cancer promotes cancer proliferation by activating the PI3K/Akt signaling pathway. *J Exp Clin Cancer Res*. 2019;38(1):497.
44. Dahlem C, Barghash A, Puchas P, Haybaeck J, Kessler SM. The Insulin-Like Growth Factor 2 mRNA Binding Protein IMP2/IGF2BP2 is Overexpressed and Correlates with Poor Survival in Pancreatic Cancer. *Int J Mol Sci*. 2019;20(13).
45. Li H, Wang D, Yi B, et al. SUMOylation of IGF2BP2 promotes vasculogenic mimicry of glioma via regulating OIP5-AS1/miR-495-3p axis. *Int J Bio Sci*. 2021;17(11):2912–2930.
46. Capel B. Vertebrate sex determination: evolutionary plasticity of a fundamental switch. *Nat Rev Genet*. 2017;18(11):675–689.
47. Ikushima H, Todo T, Ino Y, Takahashi M, Miyazawa K, Miyazono K. Autocrine TGF-beta signaling maintains tumorigenicity of glioma-initiating cells through Sry-related HMG-box factors. *Cell Stem Cell*. 2009;5(5):504–514.
48. Kuo HY, Hsu HT, Chen YC, Chang YW, Liu FT, Wu CW. Galectin-3 modulates the EGFR signalling-mediated regulation of Sox2 expression via c-Myc in lung cancer. *Glycobiology*. 2016;26(2):155–165.
49. Gangemi RM, Griffiro F, Marubbi D, et al. SOX2 silencing in glioblastoma tumor-initiating cells causes stop of proliferation and loss of tumorigenicity. *Stem Cells*. 2009;27(1):40–48.
50. Cintin C, Johansen JS, Christensen IJ, Price PA, Sørensen S, Nielsen HJ. High serum YKL-40 level after surgery for colorectal carcinoma is related to short survival. *Cancer*. 2002;95(2):267–274.
51. Diefenbach CS, Shah Z, Iasonos A, et al. Preoperative serum YKL-40 is a marker for detection and prognosis of endometrial cancer. *Gynecologic Oncol*. 2007;104(2):435–442.
52. Jensen BV, Johansen JS, Price PA. High levels of serum HER-2/neu and YKL-40 independently reflect aggressiveness of metastatic breast cancer. *Clin Cancer Res*. 2003;9(12):4423–4434.
53. Johansen JS, Brasso K, Iversen P, et al. Changes of biochemical markers of bone turnover and YKL-40 following hormonal treatment for metastatic prostate cancer are related to survival. *Clin Cancer Res*. 2007;13(11):3244–3249.
54. Junker N, Johansen JS, Andersen CB, Kristjansen PE. Expression of YKL-40 by peritumoral macrophages in human small cell lung cancer. *Lung Cancer*. 2005;48(2):223–231.
55. Tanwar MK, Gilbert MR, Holland EC. Gene expression microarray analysis reveals YKL-40 to be a potential serum marker for malignant character in human glioma. *Cancer Res*. 2002;62(15):4364–4368.
56. Colin C, Baeza N, Bartoli C, et al. Identification of genes differentially expressed in glioblastoma versus pilocytic astrocytoma using Suppression Subtractive Hybridization. *Oncogene*. 2006;25(19):2818–2826.
57. Degrauwe N, Suvá ML, Janiszewska M, Riggi N, Stamenkovic I. IMPs: an RNA-binding protein family that provides a link between stem cell maintenance in normal development and cancer. *Genes Dev*. 2016;30(22):2459–2474.
58. Douville JM, Cheung DY, Herbert KL, Moffatt T, Wagle JT. Mechanisms of MEOX1 and MEOX2 regulation of the cyclin dependent kinase inhibitors p21 and p16 in vascular endothelial cells. *PLoS One*. 2011;6(12):e29099.
59. Cao G, Huang B, Liu Z, et al. Intronic miR-301 feedback regulates its host gene, ska2, in A549 cells by targeting MEOX2 to affect ERK/CREB pathways. *Biochem Biophys Res Commun*. 2010;396(4):978–982.
60. Turcan S, Makarov V, Taranda J, et al. Mutant-IDH1-dependent chromatin state reprogramming, reversibility, and persistence. *Nature Genet*. 2018;50(1):62–72.
61. Tachon G, Masliantsev K, Rivet P, et al. Prognostic significance of MEOX2 in gliomas. *Modern Pathology*. 2019;32(6):774–786.
62. Haimeur A, Conseil G, Deeley RG, Cole SP. The MRP-related and BCRP/ABCG2 multidrug resistance proteins: biology, substrate specificity and regulation. *Curr Drug Metab*. 2004;5(1):21–53.
63. Holland PW. Evolution of homeobox genes. *WIREs Dev Biol*. 2013;2(1):31–45.
64. Murat A, Migliavacca E, Goria T, et al. Stem cell-related “self-renewal” signature and high epidermal growth factor receptor expression associated with resistance to concomitant chemoradiotherapy in glioblastoma. *J Clin Oncol*. 2008;26(18):3015–3024.
65. Duan R, Han L, Wang Q, et al. HOXA13 is a potential GBM diagnostic marker and promotes glioma invasion by activating the Wnt and TGF- β pathways. *Oncotarget*. 2015;6(29):27778–27793.
66. Li B, McCrudden CM, Yuen HF, et al. CD133 in brain tumor: the prognostic factor. *Oncotarget*. 2017;8(7):11144–11159.
67. Cai WY, Chen X, Chen LP, Li Q, Du XJ, Zhou YY. Role of differentially expressed genes and long non-coding RNAs in papillary thyroid carcinoma diagnosis, progression, and prognosis. *J Cell Biochem*. 2018;119(10):8249–8259.
68. Ye D, Jiang Y, Sun Y, et al. METTL7B promotes migration and invasion in thyroid cancer through epithelial-mesenchymal transition. *J Mol Endocrinol*. 2019;63(1):51–61.
69. Fu R, Luo X, Ding Y, Guo S. Prognostic Potential of METTL7B in Glioma. *Neuroimmunomodulation*. 2022;29(3):186–201.
70. Schiavinato A, Becker AK, Zanetti M, et al. EMILIN-3, peculiar member of elastin microfibril interface-located protein (EMILIN) family, has distinct expression pattern, forms oligomeric assemblies, and serves as transforming growth factor β (TGF- β) antagonist. *J Biol Chem*. 2012;287(14):11498–11515.
71. Xiong A, Kundu S, Forsberg-Nilsson K. Heparan sulfate in the regulation of neural differentiation and glioma development. *FEBS J*. 2014;281(22):4993–5008.

72. Zeng WJ, Yang YL, Liu ZZ, et al. Integrative Analysis of DNA Methylation and Gene Expression Identify a Three-Gene Signature for Predicting Prognosis in Lower-Grade Gliomas. *Cell Phys Biochem*. 2018;47(1):428–439.
73. Li S, Yu W, Xie F, et al. Neoadjuvant therapy with immune checkpoint blockade, antiangiogenesis, and chemotherapy for locally advanced gastric cancer. *Nat Commun*. 2023;14(1):8.
74. Watanabe N, Gavrieli M, Sedy JR, et al. BTLA is a lymphocyte inhibitory receptor with similarities to CTLA-4 and PD-1. *Nat Immunol*. 2003;4(7):670–679.
75. Cai G, Anumanthan A, Brown JA, Greenfield EA, Zhu B, Freeman GJ. CD160 inhibits activation of human CD4+ T cells through interaction with herpesvirus entry mediator. *Nat Immunol*. 2008;9(2):176–185.
76. van der Merwe PA, Bodian DL, Daenke S, Linsley P, Davis SJ. CD80 (B7-1) binds both CD28 and CTLA-4 with a low affinity and very fast kinetics. *J Exp Med*. 1997;185(3):393–403.
77. Qureshi OS, Zheng Y, Nakamura K, et al. Trans-endocytosis of CD80 and CD86: a molecular basis for the cell-extrinsic function of CTLA-4. *Science*. 2011;332(6029):6003.
78. Tan AC, Heimberger AB, Khasraw M. Immune Checkpoint Inhibitors in Gliomas. *Curr Oncol Rep*. 2017;19(4):23.
79. Hui L, Wang J, Zhang J, Long J. lncRNA TMEM51-AS1 and RUSC1-AS1 function as ceRNAs for induction of laryngeal squamous cell carcinoma and prediction of prognosis. *PeerJ*. 2019;7:e7456.
80. Hu YZ, Hu ZL, Liao TY, Li Y, Pan YL. LncRNA SND1-IT1 facilitates TGF- β 1-induced epithelial-to-mesenchymal transition via miR-124/COL4A1 axis in gastric cancer. *Cell Death Discovery*. 2022;8(1):73.
81. Zhang X, Zheng W, Jiang W, Lin R, Xing C. Long non-coding RNA SNHG3 accelerates progression in glioma by modulating miR-384/HDGF axis. *Open Life Sci*. 2020;15(1):654–664.

Cancer Management and Research

Dovepress

Publish your work in this journal

Cancer Management and Research is an international, peer-reviewed open access journal focusing on cancer research and the optimal use of preventative and integrated treatment interventions to achieve improved outcomes, enhanced survival and quality of life for the cancer patient. The manuscript management system is completely online and includes a very quick and fair peer-review system, which is all easy to use. Visit <http://www.dovepress.com/testimonials.php> to read real quotes from published authors.

Submit your manuscript here: <https://www.dovepress.com/cancer-management-and-research-journal>